Materials Chemistry and Physics, **226**, 1-5 (2019).

Electrochemical performance of a lead fluoride electrode mixed with carbon in an electrolyte containing triphenylboroxine as an anion acceptor for fluoride shuttle batteries

Hiroaki Konishi,[a, z] Taketoshi Minato,[a, z] Takeshi Abe,[b, z] and Zempachi Ogumi,[a]

[a] Office of Society-Academia Collaboration for Innovation, Kyoto University, Gokasho, Uji, Kyoto 611-0011, Japan

[b] Graduate School of Global Environmental Studies, Kyoto University, Katsura, Nishikyo, Kyoto 615-8510, Japan

[z] **Corresponding author**

Hiroaki Konishi

E-mail: hiroaki.konishi.yj@hitachi.com

Taketoshi Minato

E-mail: minato.taketoshi.5x@kyoto-u.ac.jp

Takeshi Abe

E-mail: abe@elech.kuic.kyoto-u.ac.jp

Present address

Hiroaki Konishi

Research & Development Group, Hitachi Ltd.

Hitachi, Ibaraki 319-1292, Japan

E-mail: hiroaki.konishi.yj@hitachi.com

Keywords

fluoride shuttle battery; anion acceptor; triphenylboroxine; lead fluoride

Abstract

In fluoride shuttle batteries (FSBs), the addition of an anion acceptor (AA) is required to dissolve the supporting electrolyte salt in an organic solvent. Based on theoretical calculations and practical experiments, the effectiveness of triphenylboroxine (TPhBX) as an AA for FSB was verified. Using an electrolyte with TPhBX as an AA, the specific capacities of the following two types of lead fluoride (PbF_2) electrodes were evaluated: (i) PbF_2 pulverized using a ball mill, (ii) pulverized PbF_2 mixed with carbon using a ball mill. The experimental results indicate that mixing PbF_2 with carbon using a ball mill increases the specific capacity of PbF_2 electrode.

1. Introduction

Batteries, which utilize the migration of cations such as lithium, sodium, and magnesium ions to advance the electrochemical reactions, have been widely developed [1–6]. Reddy et al. (2011) reported an all-solid-based battery that uses the migration of fluoride ions to advance the electrochemical reaction [7]. Recently, several groups began to develop batteries that use anion migration [8–14]. In these batteries, metal fluoride (MF_x; M: metal) is used as an active material, and the discharge/charge reactions proceed as follows:

Discharge: $MF_x + xe^- \rightarrow M + xF^-$

Charge: $M + xF^- \rightarrow MF_x + xe^-$

The abovementioned batteries, due to the use of a solid electrolyte, can operate at high temperatures. Contrastingly, the electrochemical performance of batteries with a liquid-based electrolyte is generally higher than the performance of batteries with a solid-based electrolyte [15, 16]. Therefore, we paid attention to liquid-based fluoride shuttle batteries (FSBs) [17–20]. The construction of a liquid-based FSB requires an electrolyte composed of organic solvents and a supporting electrolyte salt. The supporting electrolyte salt, such as cesium fluoride (CsF) is difficult to dissolve in the organic solvent (bis[2-(2-

methoxyethoxy)ethyl] ether; tetraglyme: G4), therefore, an anion acceptor (AA) was added to the G4 [17]. Although the AA addition improved the solubility of CsF, it resulted in capacity degradation during cycling due to dissolution of the active material during charging [18]. To resolve this problem, we modified the CsF concentration in the electrolyte and found that increasing the CsF concentration (saturated state) reduced the dissolution of the active material and suppressed the capacity degradation during cycling [18].

Previous studies have reported that a boroxine-based compound acts as an AA for lithium-ion batteries (LIBs) [21]. In this study, we first evaluate triphenylboroxine (TPhBX)'s ability as an AA via theoretical calculations. Secondly, we investigate TPhBX's suitability as an AA for an FSB electrolyte with practical experiments. Finally, using the electrolyte with TPhBX as an AA, we evaluate the discharge/charge capacities of the lead fluoride (PbF_2) electrode. When metal halides were used as an active material in LIBs, previous studies have reported that when mixed with carbon using a ball mill, the specific capacity of the electrodes increases [22–28]. Therefore, in this study, PbF_2 electrodes were prepared by two methods: (i) PbF_2 was pulverized using a ball mill and (ii) pulverized PbF_2 was mixed with carbon using a ball mill.

2. Theoretical calculations and experimental methods

To evaluate the effectiveness of TPhBX as an AA, the adsorption energy (*Ea*) of F^- on TPhBX was evaluated using the density functional theory (DFT) calculation as mentioned in a previous study [17]. Briefly, *Ea* was calculated using the following equation:

$$Ea = E(TPhBX–F^-) – [E(TPhBX) + E(F^-)]$$

where $E(TPhBX–F^-)$, $E(TPhBX)$, and $E(F^-)$ are the total gas-phase energies of the TPhBX–F^- complex, TPhBX molecule, and F^- anion, respectively.

Excess CsF (Tokyo Chemical Industry) was added in G4 (KISHIDA CHEMICAL) containing 0.5 mol dm^{-3} TPhBX (Tokyo Chemical Industry), which was then used as an electrolyte. The CsF concentration in the electrolyte was evaluated using atomic absorption spectrometry (AAS; Hitachi ZA3000). A three-electrode electrochemical cell (EC FRONTIER VB7) was prepared with a platinum (Pt) foil as the working electrode, a Pt mesh as the counter electrode, and a silver rod immersed in acetonitrile containing 0.1 mol dm^{-3} silver nitrate and 0.1 mol dm^{-3} tetraethylammonium perchlorate as the reference electrode (0.587 V vs. standard hydrogen electrode) [29]; a multipotentiostat (Biologic VMP-300) was used to perform cyclic voltammetry (CV) measurement of a Pt electrode in the prepared electrolyte. Three cycles were performed

between potentials of –4.0 and 2.0 V (vs. the Ag/Ag^+ reference electrode) at a sweep rate of 0.1 mV s^{-1}.

The active material was prepared according to the following method. PbF_2 (Aldrich) was pulverized in a planetary ball mill (FRITSCH PULVERISETTE 7) at 1100 rpm for 1 h. The pulverized PbF_2 is denoted by PbF_2(P). Then, 80 wt% PbF_2(P) and 20 wt% acetylene black (AB) were mixed in a planetary ball mill at 1100 rpm for 1 h, and the obtained material is denoted by PbF_2(C). A scanning electron microscope (SEM; Hitachi SU6600) equipped with an energy dispersive X-ray (EDX) analyzer (HORIBA EX-350x-act) was used to evaluate the distributions of PbF_2 and AB in PbF_2(C) powder.

The PbF_2(P) and PbF_2(C) electrodes were prepared according to the following methods. PbF_2(P) was mixed with AB and polyvinylidene difluoride (PVDF) in a proportion of 60: 25: 15 wt%. Since PbF_2(C) was composed of PbF_2 and AB (80: 20 wt%), PbF_2(C) was mixed with AB and PVDF in a proportion of 75: 10: 15 wt%. Using these electrodes as the working electrode in a three-electrode electrochemical cell, the specific capacities of PbF_2(P)/PbF_2(C) electrodes were measured over the potential range from –2.2/–2.0 to –0.6 V (vs. ref.) at 0.025C (1C = 219 mA g^{-1}). The specific capacities of both electrodes were obtained by dividing the capacity by the weight of the PbF_2. The electrolyte preparation, sealing of powders in the planetary ball mill, and electrochemical

measurements were performed at room temperature in a glove box filled with high-purity Ar.

The electronic states of Pb in each electrode during the first cycle were analyzed using X-ray photoelectron spectroscopy (XPS; ULVAC PHI Quantera SXM^{TM}) with Al Kα X-ray radiation under ultrahigh vacuum conditions. XPS spectra of the electrodes were obtained after Ar^+ sputtering (Ar^+ energy: 2 keV, ion current: 1.3 μA, and time: 16 min). The binding energies were calibrated against the Pb $4f_{7/2}$ peak of PbF_2 at 139.0 eV, and the intensities were normalized by the peak areas of the Pb $4f_{7/2}$ peaks.

3. Results and discussion

First, the effectiveness of TPhBX as an AA was evaluated using DFT calculations. Fig. 1 shows the optimized molecular structure of TPhBX–F^-. The most stable binding site for F^- is at the boron atom, and the resultant *Ea* of F^- on TPhBX is –335 kJ mol^{-1}. The *Ea* is close to that of F^- on fluorobis(2,4,6-trimethylphenyl)borane (–312.3 kJ mol^{-1}), which is used as an AA for FSB [17], suggesting that TPhBX is effective as an AA. Second, the effectiveness of TPhBX as an AA was experimentally verified. The solubility of CsF in G4 before and after addition of 0.5 mol dm^{-3} TPhBX was investigated using AAS, and the results indicate that the solubility of CsF in G4 increases

from 0.00017 to 0.51 mol dm^{-3} after TPhBX addition. Thus, the effectiveness of TPhBX as an AA for FSB is verified by both calculations and experiments.

The electrochemical stability of the prepared electrolyte during cycling was evaluated by CV (Fig. 2). A reduction peak appears below –2.2 V and a negligible oxidation peak is observed in the first cycle. The shape of CV curves changes only slightly during three cycles, indicating that the electrolyte is stable between –2.2 and 2.0 V during cycling.

Next, the extent of mixing of PbF_2 and carbon in the PbF_2(C) powder was evaluated. Previously, particles of PbF_2(C) powder were observed using SEM; however, it was difficult to evaluate the distributions of PbF_2 and AB in PbF_2(C) powder from the secondary electron image [19]. Therefore, the distributions of Pb, F, and C were evaluated using EDX in this work. Fig. 3 shows the secondary electron image and EDX mapping of Pb, F, and C. The bright area observed in the center of Fig. 3(a) is attributed to PbF_2(C), since Pb, F, and C are detected (Figs. 3(b), (c), and (d)). The bright area in which C is detected (Fig. 3(d)) overlaps with the areas in which Pb and F are detected (Figs. 3(b) and (c)), indicating that PbF_2 is adhered to AB in PbF_2(C).

Then, using the prepared electrolyte, we investigated the effects that mixing with AB have on the electrochemical performance of the PbF_2 electrode. Fig. 4 shows the

discharge and charge curves of PbF_2(P) and PbF_2(C) electrodes. Since the discharge reaction of the PbF_2(P) electrode barely proceeded above –2.0 V, the PbF_2(P) electrode was discharged to –2.2 V, which is close to the electrochemical window of the electrolyte. For the PbF_2(P) electrode (Fig. 4(a)), the first discharge capacity is similar to the theoretical capacity (219 mAh g^{-1}). However, the subsequent discharge/charge capacities are much lower than the first discharge capacity. For the PbF_2(C) electrode (Fig. 4(b)), discharge capacity in the first cycle is similar to the theoretical capacity and higher reversible capacities remain during subsequent cycles. The reversible discharge/charge capacities for PbF_2(C) (Fig. 4(b)) are much higher than those for the PbF_2(P) electrode (Fig. 4(a)). These results indicate that mixing PbF_2 with AB using a ball mill increases the reversible capacity of the PbF_2 electrode.

To clarify discharge and charge reaction differences between the PbF_2(P) and PbF_2(C) electrodes, the electronic state of Pb in each electrode during the first cycle was investigated using XPS (Fig. 5). For the PbF_2(P) electrode (Fig. 5(a)), in the pristine state, two large peaks are observed at 139.0 and 143.9 eV and two small peaks are observed at 136.6 and 141.5 eV. Four peaks are indexed to the Pb $4f_{7/2}$ and $4f_{5/2}$ peaks of PbF_2 (Pb^{2+}) and those of metallic Pb, respectively [30, 31]. Upon changing from the pristine state to the fully discharged state, peaks indexed to metallic Pb increase and peak intensities

indexed to PbF_2 decrease. From the fully discharged state to the fully charged state, the intensities of the peaks assigned to PbF_2 increase slightly and those assigned to metallic Pb decrease slightly. These results indicate that the discharge reaction partially progresses, and the charge reaction proceeds less than the discharge reaction. The first discharge capacity observed for the PbF_2(P) electrode (Fig. 4(a)) is partially attributed to side reactions such as decomposition of the electrolyte, since the discharge potential is close to the electrochemical window of the electrolyte. For the PbF_2(C) electrode (Fig. 5(b)), from the pristine state to the fully discharged state, peaks assigned to metallic Pb appear and the intensities of the peaks assigned to PbF_2 greatly decrease. From the fully discharged state to the fully charged state, peak intensities assigned to PbF_2 increase and those assigned to metallic Pb decrease. The change in the electronic state of Pb observed for the PbF_2(C) electrode was much larger than that for the PbF_2(P) electrode, indicating that the discharge/charge reactions of the PbF_2(C) electrode progress more than those of the PbF_2(P) electrode.

4. Conclusion

The ability of TPhBX as an AA was verified by theoretical calculations, and the results indicate that TPhBX can act as an AA. Then, TPhBX's effectiveness to increase

the solubility of CsF in G4 was confirmed with practical experiments. Using the electrolyte with TPhBX, the electrochemical performance of PbF_2 electrode was investigated. The discharge and charge reactions for PbF_2 can proceed using the TPhBX-containing electrolyte and the reversible capacity of PbF_2 is further improved by mixing with carbon using a ball mill. The discharge and charge reaction progress of the PbF_2 is confirmable using XPS.

Acknowledgments

This work was supported by the Research and Development Initiative for Scientific Innovation of New Generation Batteries (RISING) project from the New Energy and Industrial Technology Development Organization (NEDO), Japan. The authors thank Ms. Kiyomi Ishizawa, Ms. Ryoko Masuda, and Ms. Hisayo Ikeda for their experimental support.

References

[1] Y. Nishi, Lithium ion secondary battery; past 10 years and the future, J. Power Sources 100 (2001) 101–106.

[2] T. Minato, T. Abe, Surface and interface sciences of Li-ion batteries –Research progress in electrode-electrolyte interface-, Prog. Surf. Sci. 92 (2017) 240–280.

[3] C. Delmas, J.J. Braconnier, C. Fouassier, P. Hagenmuller, Electrochemical intercalation of sodium in Na_xCoO_2 bronzes, Solid State Ion. 3–4 (1981) 165–169.

[4] D.A. Stevens, J.R. Dahn, High Capacity Anode Materials for Rechargeable Sodium-Ion Batteries, J. Electrochem. Soc. 147 (2000) 1271–1273.

[5] T.D. Gregory, R.J. Hoffman, R.C. Winterton, Nonaqueous Electrochemistry of Magnesium, J. Electrochem. Soc. 137 (1990) 775–780.

[6] D. Aurbach, Z. Lu, A. Schechter, Y. Gofer, H. Gizbar, R. Turgeman, Y. Cohen, M. Moshkovich, E. Levi, Prototype systems for rechargeable magnesium batteries, Nature 407 (2000) 724–727.

[7] X. Zhao, Q. Li, Z. Zhao-Karger, P. Gao, K. Fink, X. Shen, M. Fichtner, Chloride ion-doped polyaniline/carbon nanotube nanocomposite materials as new cathodes for chloride ion battery, Electrohim. Acta 270 (2018) 30–36.

[8] M. A. Reddy, M. Fichtner, Batteries based on fluoride shuttle, J. Mater. Chem. 21

(2011) 17059–17062.

[9] C. Rongeat, M. A. Reddy, R. Witter, M. Fichtner, Nanostructured Fluoride-Type Fluorides As Electrolytes for Fluoride Ion Batteries, J. Phys. Chem. C 117 (2013) 4943–4950.

[10] F. Gschwind, J. Bastien, Parametric investigation of room-temperature fluoride-ion batteries: assessment of electrolytes, Mg-based anodes, and BiF_3-cathodes, J. Mater. Chem. A 3 (2015) 5628–5634.

[11] M.A. Nowroozi, K. Wissel, J. Rohrer, A.R. Munnangi, O. Clemens, $LaSrMnO_4$: Reversible Electrochemical Intercalation of Fluoride Ions in the Context of Fluoride Ion Batteries, Chem. Mater. 29 (2017) 3441–3453.

[12] X. Zhao, Z. Zhao-Karger, D. Wang, M. Fichtner, Angew. Metal Oxychlorides as Cathode Materials for Chloride Ion Batteries, Chem. Int. Ed. 52 (2013) 13621–13624.

[13] X. Zhao, Q. Li, Z. Zhao-Karger, P. Gao, K. Fink, X. Shen, M. Fichtner, Magnesium Anode for chloride Ion Batteries, Appl. Mater. Interfaces 6 (2014) 10997–11000.

[14] X. Zhao, S. Ren, M. Bruns, M. Fichtner, Chloride ion battery: A new member in the rechargeable battery family, J. Power Sources 245 (2014) 706–711.

[15] K. Takada, N. Ohta, L. Zhang, X. Xu, B. T. Hang, T. Ohnishi, M. Osada, T. Sasaki, Interfacial phenomena in solid-state lithium battery with sulfide solid electrolyte: Solid

State Ion. 225 (2012) 594–597.

[16] W. D. Richards, L. J. Miara, Y. Wang, J. C. Kim, G. Ceder, Interface Stability in Solid-State Batteries: Chem. Mater. 28 (2016) 266–273.

[17] H. Konishi, T. Minato, T. Abe, Z. Ogumi, Electrochemical Performance of a Bismuth Fluoride Electrode in a Reserve-Type Fluoride Shuttle Battery, J. Electrochem. Soc. 164 (2017) A3702–A3708.

[18] H. Konishi, T. Minato, T. Abe, Z. Ogumi, Improvement of cycling performance in bismuth fluoride electrodes by controlling electrolyte composition in fluoride shuttle batteries, J. Appl. Electrochem. 48 (2018) 1205–1211.

[19] H. Konishi, T. Minato, T. Abe, Z. Ogumi, Electrochemical properties of lead fluoride electrode in fluoride shuttle battery, J. Electroanal. Chem. 826 (2018) 60–64.

[20] H. Konishi, T. Minato, T. Abe, Z. Ogumi,Triphenylboroxine and Triphenylborane as Anion Acceptors for Electrolyte in Fluoride Shuttle Batteries, Chem. Lett. 47 (2018) 1346–1349.

[21] V.P. Reddy, M. Blanco, R. Bugga, Boron-based anion receptors in lithium-ion and metal-air batteries: J. Power Sources 247 (2014) 813–820.

[22] H. Li, P. Balaya, J. Maier, Li-Storage via Heterogeneous Reaction in Selected Binary Metal Fluorides and Oxides, J. Electrochem. Soc. 151 (2004) A1878–A1885.

[23] M. Bervas, A.N. Mansour, W.S. Yoon, J.F. Al-Sharab, F. Badway, F. Cosandey, L.C. Klein, G.G. Amatucci, Investigation of the Lithium and Delithiation Conversion Mechanisms of Bismuth Fluoride Nanocomposites, J. Electrochem. Soc. 153 (2006) A799–A808.

[24] N. Yabuuchi, M. Sugano, Y. Yamakawa, I. Nakai, K. Sakamoto, H. Muramatsu, S. Komaba, Effect of heat-treatment process on FeF_3 nanocomposite electrodes for rechargeable Li Batteries, J Mater. Chem. 21 (2011) 10035–10041.

[25] M.A. Reddy, B. Breitung, C. Wall, S. Trivedi, V. Sai, K. Chakravadhanula, M. Helen, M. Fichtner, Facile Synthesis of Carbon-Metal Fluoride Nanocomposites for Lithium-Ion Batteries, Energy Technol. 4 (2016) 201–211.

[26] H. Konishi, T. Minato, T. Abe, Z. Ogumi, Cycling Fading Mechanism for a Bismuth Fluoride Electrode in a Lithium-Ion Battery, Chemistry Select 2 (2017) 3504–3510.

[27] H. Konishi, T. Minato, T. Abe, Z. Ogumi, Electrochemical Reaction Mechanism for $Bi_{1-x}Ba_xF_{3-x}$ (x = 0, 0.1, 0.2, and 0.4) Electrodes in Lithium-Ion Batteries, Chemistry Select 2 (2017) 6399–6406.

[28] H. Konishi, T. Minato, T. Abe, Z. Ogumi, Difference of rate performance between discharge and charge reactions for bismuth fluoride electrode in lithium-ion battery, J. Electroanal. Chem. 806 (2017) 82–87

[29] V.V. Pavlishchuk, A.W. Addison, Inorg. Conversion constants for redox potentials measured versus different reference electrodes in acetonitrile solutions at 25°C, Chim. Acta 298 (2000) 97–102.

[30] B. Huang, J.M. Hong, X.T. Chen, Z.L. Xue, X.Z. You, Room temperature selective preparation and characterization of nanorods $PbF_{2(1-x)}Br_{2x}$ (x = 0.15, 0.3), J. Crystal Growth 276 (2005) 491–497.

[31] H. Li, G. Zhang, L. Wang, Low humidity-sensitivity of MoS_2/Pb nanocomposite coatings, Wear 350–351 (2016) 1–9.

Figures

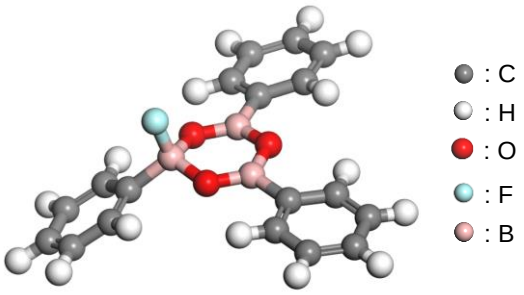

Fig. 1. Optimized molecular structure of TPhBX–F^-.

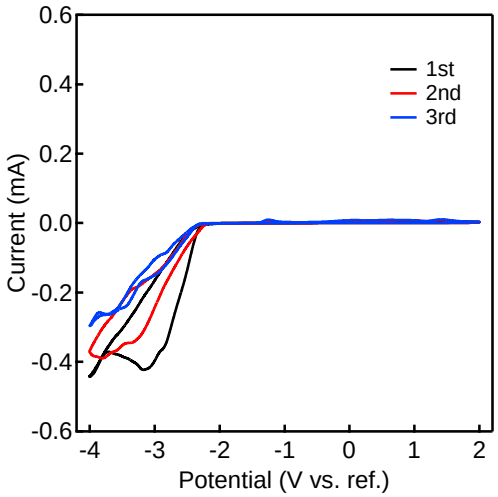

Fig. 2. Cyclic voltammograms of a Pt electrode immersed in an electrolyte during three cycles.

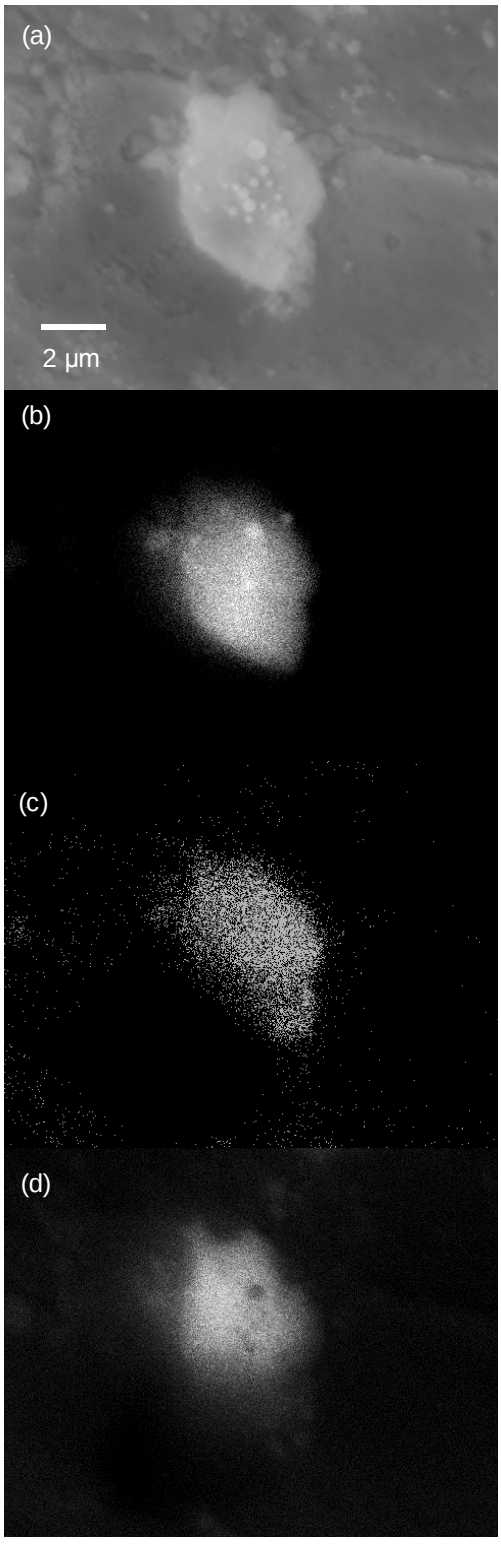

Fig. 3. (a) Secondary electron image and EDX mapping of (b) Pb, (c) F, and (d) C for PbF_2(C) powder.

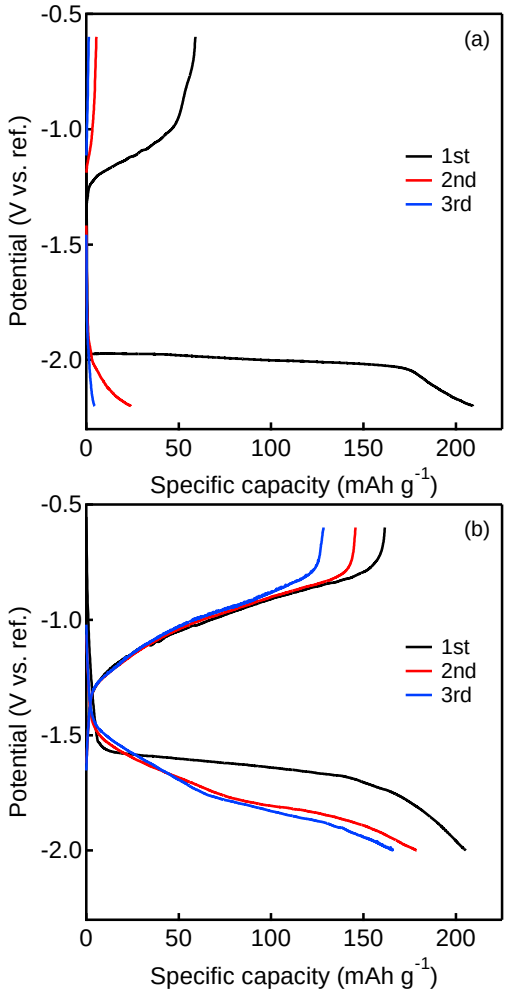

Fig. 4. Discharge and charge curves of the (a) PbF_2(P) and (b) PbF_2(C) electrodes during three cycles.

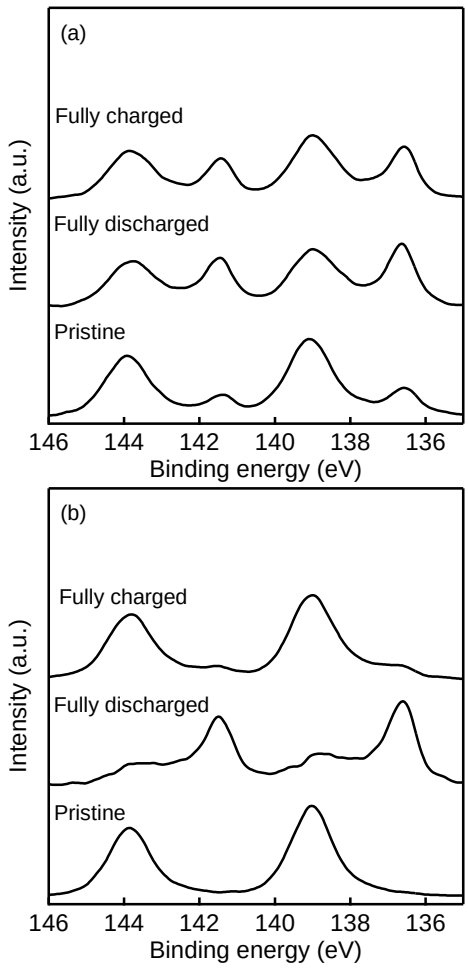

Fig. 5. Pb 4f XPS spectra of (a) PbF_2(P) and (b) PbF_2(C) electrodes in the pristine, fully discharged, and fully charged states during the first cycle.